Progress In Electromagnetics Research C, Vol. 22, 165–178, 2011

DESIGN OF CONCURRENT LOW-NOISE AMPLIFIER FOR MULTI-BAND APPLICATIONS

G.-L. Ning*, Z.-Y. Lei, L.-J. Zhang, R. Zou, and L. Shao

National Laboratory of Antennas and Microwave Technology, Xidian University, Xi'an, Shaanxi 710071, P. R. China

Abstract—A concurrent multi-band low-noise amplifier (LNA) for both WLAN and WiMAX applications covering 2.4–2.7 GHz, 3.3–3.8 GHz and 5.1–5.9 GHz is mainly investigated. The proposed LNA consists of two cascaded common-source stages and employs stepped-impedance transformers and series and shunt feedback techniques to obtain good return loss, low noise and high linearity simultaneously. Test results show that the LNA features input and output return loss of 12 dB, gain of 21 dB, and noise figure of 2 dB across the three bands of operation, which are the state of the art among the counterparts.

1. INTRODUCTION

With the development of wireless communications, requirements for transceivers that can support multi-bands and multi-standards, such as WLAN, Wi-Fi, Bluetooth, WiMAX, and ultra-wideband (UWB), are continuously increasing [1]. One of the key bottlenecks for multiple-standard communications is the implementation of the low-noise amplifier (LNA) that can operate at different frequency bands, which plays an important role in the noise performance or sensitivity of the total receiver chain. The challenges include a good input matching, flat frequency response of power gain, low noise figure (NF), and sufficient high linearity within the desired bands. A straightforward approach implements multiple separated narrowband amplifiers, each designed for a different frequency band [2, 3]. Apparently this method suffers from high power dissipation, a large chip area and therefore a significant increase in cost. Recently the switched or

Received 24 May 2011, Accepted 24 June 2011, Scheduled 30 June 2011

* Corresponding author: Gao-Li Ning (gln429@126.com).

reconfigurable LNAs by capacitors, inductors, transistors or RF micro electro mechanical systems (MEMS) have also been reported [4–9]. However, this degrades the noise figure, and only one band can be selected at a time. The wide-band LNAs that cover the bands of interest are alternative while strong unwanted blockers are amplified together with the desired frequency bands and significantly degrade the receiver's sensitivity [10–17]. To circumvent the above problems, concurrent LNAs were developed [18–24]. The concurrent LNAs enable simultaneous multi-band operations in the same circuitry, and therefore present lower power consumption and reduced chip area. It should also be noted that multiple bands handling capability is the main drawback for this concept, which makes the linearity significant for this situation.

In this study, a concurrent triple-band LNA suitable for both WLAN and WiMAX applications covering 2.4–2.7 GHz, 3.3–3.8 GHz and 5.1–5.9 GHz is investigated as one of the alternatives to alleviate the above-mentioned problems. Compared to the prior concurrent LNAs, triple distinct bands of operation, lower NF and higher linearity are obtained. The design methodology is detailed in the following sections. Section 2 describes simultaneous noise and input impedance matching resulted from the source degenerated structure, the frequency response shaped by the stepped-impedance transformer, and the new shunt-feedback circuit. Moreover, the results and discussion of the LNA are reported in Section 3. Finally, Section 4 concludes this work.

2. CIRCUIT DESIGN

In this work, we choose not to use additional circuit techniques such as cascode structure or differential cross-coupling, as it is our goal to treat the design in a general fashion. These techniques optimize the performance to some extent, but add little to the essence of the approach. As we will show, even without these tricks, the presented design achieves state-of-the-art performances. Overall, the simplicity of the circuit is a benefit, as it reduces the number of sources for parasitic capacitance, noise and distortion. The schematic diagram of the proposed LNA is shown in Figure 1. It can be decomposed into three parts: the inductively degenerated input stage; the output stage with shunt feedback; the input, inter-stage and output matching networks MN_1, MN_2 and MN_3. The proposed design is simulated and optimized with Advanced Design System (ADS) from Agilent Technologies.

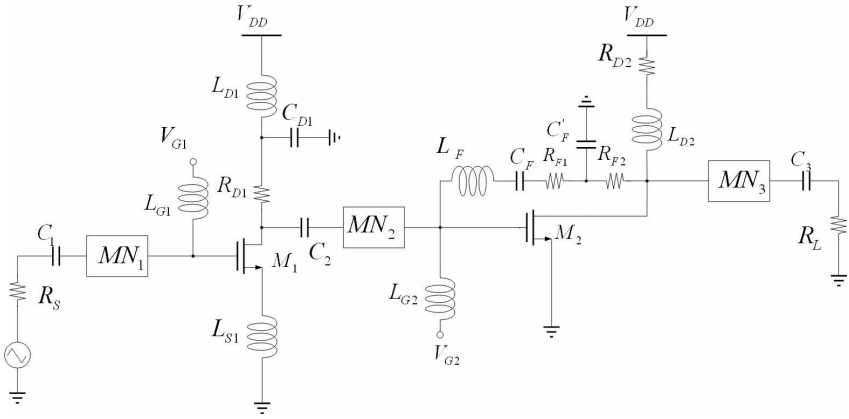

Figure 1. Schematic diagram of the proposed LNA.

2.1. Inductively Degenerated Input Stage

The input stage, which is mainly designed for low noise consideration, consists of a common-source amplifier with an additional source inductor. The source inductor L_{S1} is added for simultaneous input impedance and noise matching as discussed below.

From the small-signal equivalent circuit of the LNA (not shown here), without L_{S1}, the input impedance Z_{in} looking into the gate of the transistor M_1 is

$$Z_{in} = r - j\frac{1}{\omega C_{gs1}} \tag{1}$$

where r represents the loss in the gate of the transistor M_1, C_{gs1} is the gate-source capacitance of M_1 [23]. Although in our analysis here the effect of the gate-drain capacitance C_{gd1} of M_1 is neglected, the simplified analysis still provides a useful and quick assessment. Typically, r and C_{gs1} take on the values of less than 10 Ohm and a few tenths of a pF, respectively, which leads to a significant distance between Z_{in}^* and Γ_{opt} (the optimum source reflection coefficient for minimum NF) on the Smith chart since the real part of input impedance is too small and the imaginary part is more capacitive than needed [25]. While L_{S1} is added to the source of M_1, the input impedance Z'_{in} becomes

$$Z'_{in} = r + g_{m1}\frac{L_{S1}}{C_{gs1}} + j\left(\omega L_{S1} - \frac{1}{\omega C_{gs1}}\right) \tag{2}$$

where g_{m1} is the transconductance of M_1. As can be seen from (2), the source degeneration brings an increase in the real part at the

input impedance. However, the noise parameters including Γ_{opt} remain relatively undisturbed because of the nature of being lossless of L_{S1}. Therefore, if not excessive, L_{S1} shifts Z_{in}^* closer to Γ_{opt}, which means a simultaneous input impedance and noise matching could be obtained.

To demonstrate our conclusion further, the real parts of the input impedance Z_{in1} and Z_{in2} before and after L_{S1} of 0.3 nH is added are both plotted in Figure 2. Clearly, the input resistance increases by about 15 Ω with the addition of L_{S1}. Moreover the real part of the input impedance keeps approximately constant with frequency, which is in accordance with those given in Equations (1) and (2). In addition, the source reflection coefficient Γ_s corresponding to Z_{in}^* and Γ_{opt} at different frequencies before and after L_{S1} is added are shown in Table 1. It is found that: (1) there is only a slight variation in Γ_{opt} after L_{S1} is added; (2) with the addition of L_{S1}, Γ_s is much closer to Γ_{opt} indeed. Both the results confirm the analysis above further.

It should be noted that the stability of the amplifier is also enhanced due to the increase in the real part of the input impedance. Certainly, the penalty is the reduced gain.

Depicted in Figure 3 is the equivalent circuit of the input stage for noise analysis. As the frequency goes higher, the gain of M_1 becomes low, and the output noise power contributed by R_S and M_1 is abated;

Table 1. Comparison of Γ_s and Γ_{opt} with and without the addition of L_{S1}.

(a) Without L_{S1}.

Frequency (GHz)	2.4	2.7	3.1	3.3
Γ_s (Mag./Phase)	0.63/−3.1°	0.63/−3.0°	0.64/−2.8°	0.64/−2.7°
Γ_{opt} (Mag./Phase)	0.20/−3.1°	0.26/−2.9°	0.33/−2.7°	0.36/−2.5°
Frequency (GHz)	3.8	5.1	5.5	5.9
Γ_s (Mag./Phase)	0.66/−2.5°	0.71/ − 2.1°	0.72/−2.0°	0.74/−1.8°
Γ_{opt} (Mag./Phase)	0.44/−2.3°	0.50/−2.2°	0.63/−1.8°	0.66/−1.7°

(b) With L_{S1}.

Frequency (GHz)	2.4	2.7	3.1	3.3
Γ_s (Mag./Phase)	0.32/−2.9°	0.32/−2.8°	0.33/−2.5°	0.35/−2.4°
Γ_{opt} (Mag./Phase)	0.20/−3.0°	0.27/−2.6°	0.34/−2.4°	0.38/−2.2°
Frequency (GHz)	3.8	5.1	5.5	5.9
Γ_s (Mag./Phase)	0.39/−2.4°	0.61/−1.9°	0.59/−2.1°	0.65/−1.6°
Γ_{opt} (Mag./Phase)	0.46/−2.1°	0.45/−2.2°	0.65/−1.6°	0.70/−1.5°

therefore, R_{D1} plays a critical role in increasing the noise figure [26]. Here we assume that the impedance seen looking into the drain of M_1 is equal to Z_0, the impedance of parallel-LC circuit is Z_{LC}, and then the output noise power contributed by R_{D1} can be derived as

$$V_{n,o1}^2 = 4kTR_{D1} \times \frac{Z_0^2}{(Z_0 + R_{D1} + Z_{LC})^2} \tag{3}$$

where k is the Boltzmann constant, T is the absolute temperature, respectively. From (3), $V_{n,o1}^2$ is inversely proportional to Z_{LC}, so the output noise can be effectively reduced at the antiresonance of L_{D1} and C_{D1}.

The value of the drain inductor L_{D1} must be judiciously selected for its twofold function. First it improves the noise performance at

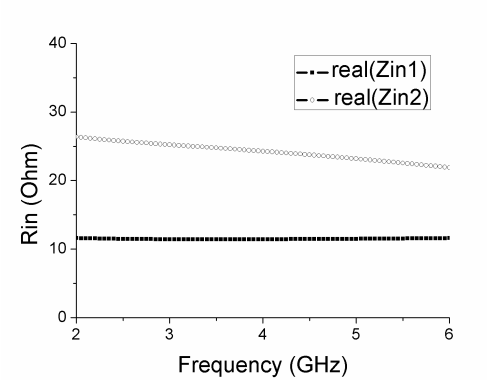

Figure 2. Change of the real part of the input impedance.

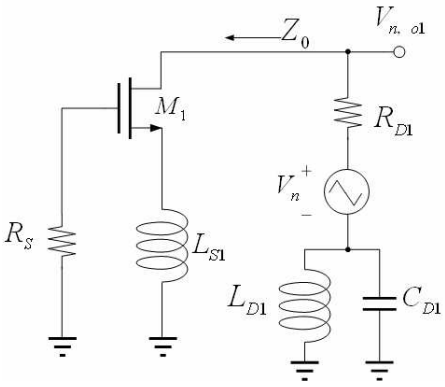

Figure 3. Equivalent circuit for suppressing the thermal noise of R_{D1}.

high frequencies for its resonance with the capacitor C_{D1} as discussed above, which will also be seen as a small dip in NF around 5.7 GHz (shown in Figure 7). What's more, L_{D1} and the series resistor R_{D1} are designed to have a peaking characteristic to compensate the gain roll-off of the devices at high frequencies. In this design, L_{D1}, R_{D1} and C_{D1} are optimized as 5 nH, 25 Ω and 1 pF, respectively.

2.2. Output Stage with Shunt Feedback

The output stage is a common-source amplifier with a shunt feedback from drain to gate. This stage aims at high linearity with additional gain enhancement. This shunt feedback is just from the drain of the transistor M_2 to its gate rather than to the input of the whole LNA, which would deteriorate the overall noise performance significantly. The feedback resistor R_F must be chosen with the trade-off between the bandwidth, linearity and gain. C_F is for DC blocking and L_F is for decreasing the feedback at high frequency, respectively. The new feedback circuit proposed here is demonstrated to improve not only the flatness of the gain, bandwidth and linearity but also the stability. The values of L_F, C_F, R_F, C'_F, R_{F2} in this design are 8 nH, 0.4 pF, 100 Ω, 0.2 pF, 150 Ω, respectively.

2.3. Matching Networks

To obtain the maximum gain as possible, the whole LNA is fully matched, which means the input, output and inter-stage matching network are required to accomplish conjugate matching for each stage. The detailed matching principle of covering three bands simultaneously is expounded as follows.

As illustrated in Figure 4, the stepped-impedance transformer is composed of n sections, each of them with a characteristic impedance Z_i and physical length l_i, where the subscript denotes the i-th section.

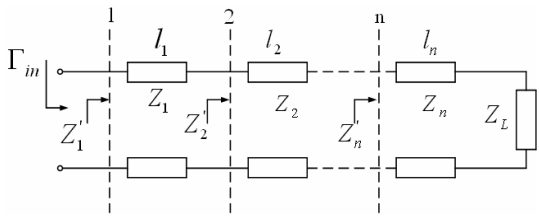

Figure 4. Principle of multi-band matching by stepped-impedance transformer.

It is terminated with a load impedance Z_L, which is frequency dependent to imitate the input/output impedance of each stage. The impedance Z'_i seen looking toward the termination at the left hand of each section is

$$Z'_i = Z_i \frac{Z'_{i+1} + jZ_i \tan(\beta l_i)}{Z_i + jZ'_{i+1} \tan(\beta l_i)} \tag{4}$$

with $i = 1, 2, \ldots, n$, β being the propagation constant. By using (4) recursively we can then obtain the input reflection coefficient Γ_{in}, as a function of Z_i and l_i,

$$\Gamma_{in} = \frac{Z'_1 - Z_0}{Z'_1 + Z_0} \tag{5}$$

with Z_0 the reference impedance. To match this frequency-dependent termination to the system impedance at given design frequencies, $\Gamma_{in} = 0$ should hold at each desired frequency, and hence a set of m nonlinear complex-valued equations is formed, where m is the number of the design frequencies. As long as $n \geq m$ as well as Z_i and l_i being free variables is ensured, the set of equations is solvable, and accordingly our goal is achieved. For the preliminary solution, the formula in [27] may be a good reference, which can be further optimized for the optimal performances of the whole LNA by a simulator. To obtain a wide band, each matching network has 5 sections, with the specific values in Table 2 and the subscripts numbered from left to right according to Figure 1. Note this inductorless matching technique also helps to achieve superior noise performance.

Table 2. Design values of the stepped-impedance transformer.

(a) Input matching network.

Number	1	2	3	4	5
Width (mm)	0.8	1.0	5.7	0.1	8.3
Length (mm)	5.1	8.0	1.8	1.9	2.8

(b) Inter-stage matching network.

Number	1	2	3	4	5
Width (mm)	0.1	4.1	0.1	0.1	8.6
Length (mm)	1.6	3.7	9.5	5.2	1.6

(c) Output matching network.

Number	1	2	3	4	5
Width (mm)	5.5	6.0	0.4	9.5	8.4
Length (mm)	9.7	8.1	0.9	1.9	0.2

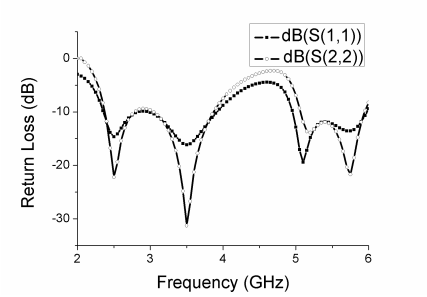

Figure 5. Input and output return loss of the LNA.

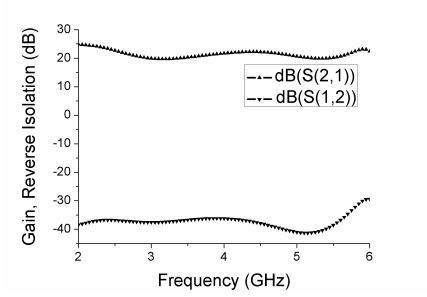

Figure 6. Gain and reverse isolation of the LNA.

3. RESULTS AND DISCUSSION

The device is chosen as ATF-54143, in enhancement-mode GaAs pHEMT technology, and the model used is Advanced curtice 2, both from Avago Technologies. Other capacitor and inductor components are with chip packing from Murata Manufacturing Co., Ltd.. The whole LNA is on an FR-4 PCB board with a relative dielectric constant ε_r of 4.4 and thickness of 0.8 mm and draws 20 mA from the 2-V supply. Since this design mainly focuses on low noise, good input/output return loss and high linearity with triple-band operation, the power consumption here is somewhat larger than those especially in CMOS technology. The one-tone and two-tone test are performed here to demonstrate the return loss, gain, reverse isolation, noise figure and the input third-order intercept point (IIP3) for linearity, respectively, which are illustrated in Figures 5–9. As can be seen from Figure 5, the input and output return losses are both better than 12 dB across 2.4–2.7 GHz, 3.3–3.8 GHz and 5.1–5.9 GHz for simultaneous WLAN and WiMAX applications, which demonstrates a successful design of our stepped-impedance as the input, output and inter-stage matching network. In Figure 6, the power gain ranges from 20 to 24 dB over the triple bands of interest, which is attributed to the shunt peaking and feedback. Reverse isolation is an important consideration in the design of amplifiers as poor reverse isolation may lead to oscillation. This issue

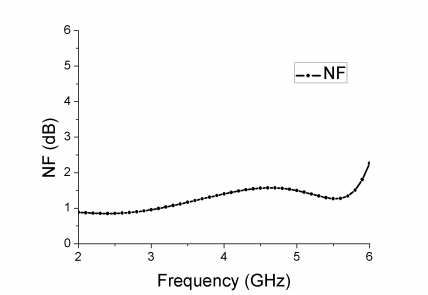

Figure 7. Noise figure of the LNA.

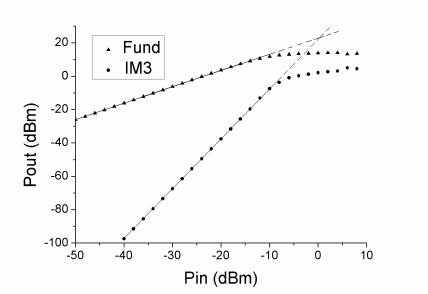

Figure 8. IIP3 of the LNA at 5.2 GHz.

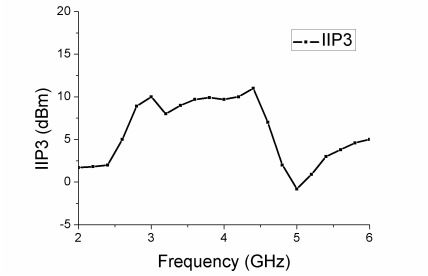

Figure 9. IIP3 of the LNA vs. frequency.

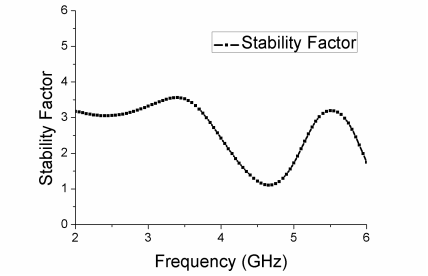

Figure 10. Stability of the LNA vs. frequency.

is particularly concerned for feedback amplifiers due to high possibility of severely poor isolation caused by the feedback itself. As seen in Figure 6, S_{12} keeps below -30 dB within the desired bands, which suggests that the shunt feedback technique doesn't do much damage to the reverse isolation of the LNA. As shown in Figure 7, the NF stays below 2 dB from 2 GHz to 5.9 GHz with a small dip around 5.7 GHz due to the antiresonance. The linearity of the proposed LNA is checked by feeding two tones with 1 MHz spacing, with the IIP3 of 1 dBm at 5.2 GHz illustrated in Figure 8. The dependence of IIP3 on frequency is also depicted in Figure 9. Due to the feedback configuration, the developed LNA has a good linearity, varying from -1 to 11 dBm across 2–6 GHz. To the authors' knowledge, the noise performance and the linearity are the sate of the art among the published work. Figure 10 shows the stability factor extracted from the two-port S parameters to estimate the stability of the LNA. Apparently it keeps larger than one across the three working bands, which indicates an unconditionally

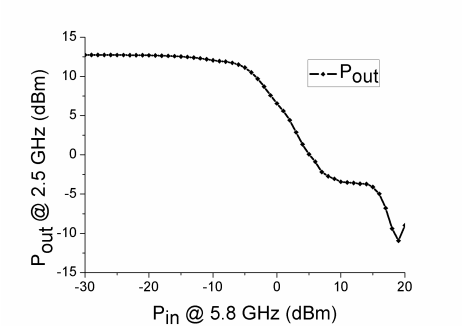

Figure 11. Signal compression with increase of signals in other bands.

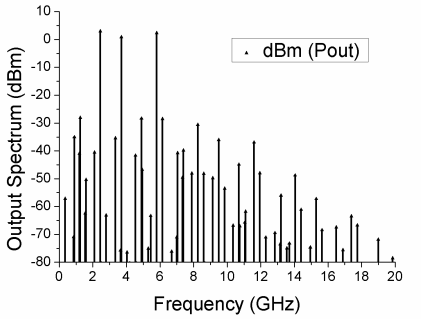

Figure 12. Output spectrum with simultaneous 3-band signal input.

stable design.

A study of the performance degradation in one band when there is signal in another band has been made. Here we apply two signals with −10 dBm level at 2.5 GHz and 5.8 GHz to the LNA. Figure 11 plots the relationship between the output signal at 2.5 GHz and the level of the input signal at 5.8 GHz. As seen, with the signal at 5.8 GHz at the input increasing, the output signal at 2.5 GHz is gradually compressed. When large enough, it is nearly blocked, as known the large signal blocking effect. The performance of the LNA under simultaneous 3-band signal input is also studied. As shown in Figure 12, with signals at 2.5 GHz, 3.5 GHz and 5.8 GHz all with −20 dBm level applied to the input simultaneously, each signal is amplified almost without compression due to interference from others and all the spurious output are below −28 dBm, thus proving the feasibility of the proposed LNA.

Table 3 gives a summary of the results of this work and the recently published concurrent multi-band LNAs. As can be seen, this work features low NF, high IIP3 as well as good input/output return loss and performs pretty well.

The design technique presented in this study can be easily applied to other LNAs with multi-band operation. As a demonstration, a concurrent dual-band LNA for WLAN applications according to 802.11 b/a/g standards to cover 2.4/5.2/5.8 GHz bands is also designed. The corresponding S parameters are illustrated in Figure 13, with input/output return loss better than 13 dB, gain about 22 dB, reverse isolation better than 30 dB across 2.4–2.5 GHz, 5.1–5.9 GHz. Noise and linearity performances are comparable to the former LNA proposed. Apparently, satisfied results are achieved once again.

Table 3. Comparison of present work and previously reported works.

Parameters	[19]		[22]		[18]		
Technology	CMOS		SiGe HBT		CMOS		
f_0 (GHz)	2.4	5.2	2.4	5.2	2.4	3.5	5.2
S_{11} (dB)	−13.5	−13.2	−22.4	−12.3	−10.37	−10.41	−13.56
S_{22} (dB)	−18.2	−7.3	−13.7	−13	−12.47	−12.17	−19.32
S_{21} (dB)	14.2	14.6	24.6	15.8	11.79	11.7	10.03
NF (dB)	4.4	3.7	2.41	3.4	3.89	4.03	3.73
IIP3 (dBm)	−3.4	−2.7	−19.9	−12	−3	−2.1	−0.4
DC supply	6 mA, 1.2 V		9 mA, 1.2 V		10 mA, 1.4 V		
Parameters	[23]		[24]		This work		
Technology	GaAs pHEMT		GaAs E-pHEMT		GaAs E-pHEMT		
f_0 (GHz)	2.4	5.8	2.4	5.8	2.4	3.5	5.5
S_{11} (dB)	−8.5	−21.6	−7.2	−8.3	−14.7	−16.2	−13.6
S_{22} (dB)	−10.1	−11.8	−9.1	−14.8	−22.2	−31.3	−13.7
S_{21} (dB)	12.2	15.3	16.8	17.7	22.4	21.1	20.7
NF (dB)	0.53	1.43	1.5	1.7	0.9	1.2	1.3
IIP3 (dBm)	N. A.		−2.8	−1.7	4.3	9.2	3.5
DC supply	10 mA, 4 V		18 mA, 1.4 V		20 mA, 2 V		

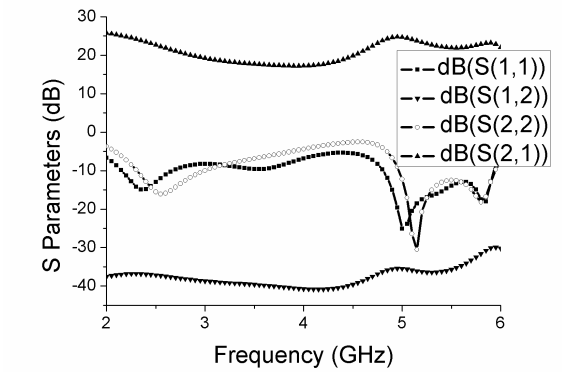

Figure 13. S parameters of the dual-band LNA for WLAN applications.

4. CONCLUSION

This work investigates a novel circuit topology of concurrent multi-band LNA for both WLAN and WiMAX applications. By the stepped-impedance transformer and feedback techniques, excellent performances including input and output return loss of 12 dB, gain of 21 dB, and noise figure of 2 dB are achieved across the three bands of operation. Such design for WLAN/WiMAX applications is the first of its kind and the state-of-the-art performances distinguish the LNA in future multi-band applications.

ACKNOWLEDGMENT

The financial support of this study by the National Natural Science Foundation of China under Grant 60771040 is appreciated. The authors are also thankful to the Microwave Research Institute for the hardware and software support.

REFERENCES

1. Hashemi, H. and A. Hajimiri, "Concurrent multiband low-noise amplifiers — Theory, design, and applications," *IEEE Trans. Microw. Theory Tech.*, Vol. 50, No. 1, 288–301, 2002.
2. Perumana, B. G., J. C. Zhan, S. S. Taylor, B. R. Carlton, and J. Laskar, "Resistive-feedback CMOS low-noise amplifiers for multiband applications," *IEEE Trans. Microw. Theory Tech.*, Vol. 56, No. 5, 1228–1225, 2008.
3. Phansathitwong, K., H. Sjoland, and P. Andreani, "Low power multi-band CMOS receiver front-end," *Proc. PRIME Conf.*, 1–4, 2010.
4. Okazaki, H., K. Kawai, A. Fukuda, T. Furuta, and S. Narahashi, "Reconfigurable amplifier towards enhanced selectivity of future multi-band mobile terminals," *International Microwave Workshop Series on RF Front-ends for Software Defined and Cognitive Radio Solutions*, 1–4, 2010.
5. Malmqvist, R., P. Rantakari, C. Samuelsson, M. Lahti, S. Cheng, and J. Saijets, "RF MEMS based impedance matching networks fortunable multi-band microwave low noise amplifiers," *Proc. International Semiconductor Conf.*, 303–306, 2009.
6. Phan, A.-T. and R. Farrell, "Reconfigurable multiband multimode LNA for LTE/GSM, WiMAX, and IEEE 802.11.a/b/g/n," *Proc. Electronics, Circuits, and Systems Conf.*, 78–81, 2010.

7. Tzeng, F., A. Jahanian, and P. Heydari, "A multiband inductor-reuse CMOS low-noise amplifier," *IEEE Transactions on Circuits and Systems — II: Express Briefs*, Vol. 55, No. 3, 209–213, 2008.
8. Lu, L.-H., H.-H. Hsieh, and Y.-S. Wang, "A compact 2.4/5.2-GHz CMOS dual-band low-noise amplifier," *IEEE Microwave and Wireless Components Letters*, Vol. 15, No. 10, 685–687, Oct. 2005.
9. Chang, S.-F., W.-L. Chen, and C.-H. Hsu, "CMOS dual-band variable-gain amplifier for 3G-WCDMA and WLAN dual-mode RF receivers," *Electronics Letters*, Vol. 43, No. 2, 102–103, Jan. 2007.
10. Li, J.-Y., W.-J. Lin, M.-P. Houng, and L.-S. Chen, "A compact wideband matching 0.18-μm CMOS UWB low-noise amplifier using active feedback technique," *Progress In Electromagnetics Research C*, Vol. 16, 161–169, 2010.
11. Hsieh, J.-Y., T. Wang, and S.-S. Lu, "Wideband low-noise amplifier by LC load-reusing technique," *Electronics Letters*, Vol. 45, No. 25, 1280–1281, 2009.
12. Dorafshan, A. and M. Soleimani, "High-gain CMOS low noise amplifier for ultra wide-band wireless receiver," *Progress In Electromagnetics Research C*, Vol. 7, 183–191, 2009.
13. Wang, C.-H., Y.-T. Chiu, and Y.-S. Lin, "3.1 dB NF 20–29 GHz CMOS UWB LNA using a T-match input network," *Electronics Letters*, Vol. 46, No. 19, 1312–1313, 2010.
14. Wong, S.-K., F. Kung Wai Lee, S. Maisurah, M. N. B. Osman, and S. J. Hui, "Design of 3 to 5 GHz CMOS low noise amplifier for ultra-wideband (UWB) system," *Progress In Electromagnetics Research C*, Vol. 9, 25–34, 2009.
15. Yoon, J., H. Seo, I. Choi, and B. Kim, "Wideband LNA using a negative GM cell for improvement of linearity and noise figure," *Journal of Electromagnetic Waves and Applications*, Vol. 24, Nos. 5–6, 619–630, 2010.
16. Ismail, A. and A. A. Abidi, "A 3–10-GHz low-noise amplifier with wideband LC-ladder matching network," *IEEE Journal of Solid-State Circuits*, Vol. 39, No. 12, 2269–2277, Dec. 2004.
17. Sapone, G. and G. Palmisano, "A 3–10-GHz low-power CMOS low-noise amplifier for ultra-wideband communication," *IEEE Trans. Microw. Theory Tech.*, Vol. 59, No. 3, 678–686, Mar. 2011.
18. Kao, C.-Y., Y.-T. Chiang, and J.-R. Yang, "A concurrent multi-band low-noise amplifier for WLAN/WiMAX applications," *Proc. International Electro. Information Technology Conf.*, 514–517, 2008.

19. Wang, S. and B.-Z. Huang, "A high-gain CMOS LNA for 2.4/5.2-GHz WLAN applications," *Progress In Electromagnetics Research C*, Vol. 21, 155–167, 2011.
20. Lin, Y.-T. and S.-S. Lu, "A 2.4/3.5/4.9/5.2/5.7-GHz concurrent multiband low noise amplifier using InGaP/GaAs HBT technology," *IEEE Microwave and Wireless Components Letters*, Vol. 14, No. 10, 463–465, Oct. 2004.
21. Fagotti, R., A. Cidronali, and G. Manes, "Concurrent hex-band GaN power amplifier for wireless communication systems," *IEEE Microwave and Wireless Components Letters*, Vol. 21, No. 2, 89–91, 2011.
22. Lin, Y.-S. and K.-N. Liao, "A concurrent multiband SiGe LNA for 1.8/1.9-GHz GSM, 2.4/5.2/5.7-GHz WLAN, and 5–7-GHz UWB system applications," *Microw. Optical Technol. Lett.*, Vol. 47, No. 1, 36–41, Oct. 2005.
23. Duo, X.-Z., L.-R. Zheng, M. Ismail, and H. Tenhunen, "A concurrent multi-band LNA for multi-standard radios," *Proceedings of the International Symposium on Circuits and Systems*, 3982–3985, May 2005.
24. Zulfa, H.-A., Y.-H. Chow, and Y. W. Eng, "A low-voltage, fully-integrated (1.5–6) GHz low-noise amplifier in E-mode pHEMT technology for multiband, multimode applications," *Proc. European Microwave Integrated Circuits Conf.*, 306–309. 2008.
25. Nguyen, T.-K., C.-H. Kim, G.-J. Ihm, M.-S. Yang, and S.-G. Lee, "CMOS low-noise amplifier design optimization techniques," *IEEE Trans. Microw. Theory Tech.*, Vol. 52, No. 5, 1433–1442, 2004.
26. He, K.-H., M.-T. Li, C.-M. Li, and J.-H. Tarng, "Parallel-RC feedback low-noise amplifier for UWB applications," *IEEE Transactions on Circuits and Systems — II: Express Briefs*, Vol. 57, No. 8, 582–586, 2010.
27. Liu, X., Y. Liu, S. Li, F. Wu, and Y. Wu, "A three-section dual-band transformer for frequency-dependent complex load impedance," *IEEE Microwave and Wireless Components Letters*, Vol. 19, No. 10, 611–613, 2009.